Mass-temperature relation in ΛCDM and modified gravity

Antonino Del Popolo,[1,2,*] Francesco Pace,[3,†] and David F. Mota[4,‡]

[1]*Dipartimento di Fisica e Astronomia, University of Catania, Via S. Sofia 64, 95123 Catania, Italy*
[2]*INFN sezione di Catania, Via S. Sofia 64, I-95123 Catania, Italy*
[3]*Jodrell Bank Centre for Astrophysics, School of Physics and Astronomy, The University of Manchester, Manchester M13 9PL, United Kingdom*
[4]*Institute of Theoretical Astrophysics, University of Oslo, P.O. Box 1029 Blindern, N-0315 Oslo, Norway*

(Received 22 January 2019; published 10 July 2019)

We derive the mass-temperature relation using an improved top-hat model and a continuous formation model which takes into account the effects of the ordered angular momentum acquired through tidal-torque interaction between clusters, random angular momentum, dynamical friction, and modifications of the virial theorem to include an external pressure term usually neglected. We show that the mass-temperature relation differs from the classical self-similar behavior, $M \propto T^{3/2}$, and shows a break at 3–4 keV and a steepening with a decreasing cluster temperature. We then compare our mass-temperature relation with those obtained in the literature with N-body simulations for $f(R)$ and symmetron models. We find that the mass-temperature relation is not a good probe to test gravity theories beyond Einstein's general relativity, because the mass-temperature relation of the ΛCDM model is similar to that of the modified gravity theories.

DOI: 10.1103/PhysRevD.100.024013

I. INTRODUCTION

The wealth of astronomical observations available nowadays clearly shows either that our Universe contains more mass-energy than is seen or that the accepted theory of gravity, general relativity (GR), is somehow not correct, or both [1]. The central assumption of the concordance ΛCDM model relies on gravity being correctly described by GR so that dark matter (DM), a nonbaryonic and nonrelativistic particle, and dark energy (DE), in the form of the cosmological constant Λ, constitute its dominant components [2]. Despite gravitational evidence for DM from galaxies [3], cluster of galaxies [4], cosmic microwave background (CMB) anisotropies [5], cosmic shear [6], structure formation [7], and large-scale structure of the Universe [8], decades of direct and indirect searches of those DM particles did not give any positive result [9]. In addition, the accelerated expansion of the universe modeled with Λ [10] raised the "cosmological constant fine-tuning problem" and the "cosmic coincidence problem" [11–13].

The success of the ΛCDM model in describing the formation and evolution of the large-scale structures in the Universe at early and late times [7,14,15] cannot hide the tensions at small [16–22] and large scales [23–29] precision data are currently revealing.

Small-scale problems [22] have sprung two sets of attempts of solutions to save the ΛCDM paradigm: cosmological and astrophysical recipes. The first are based on either modifying the power spectrum on small scales [30] or altering the kinematic or dynamical gravitational behavior of the constituent DM particles. The latter, like supernovae feedback [22,31,32] and transfer of energy and angular momentum from baryon clumps to DM through dynamical friction [33–37], rely on some "heating" mechanism producing an expansion of the galaxy's DM component which reduces its inner density.

The previous issues seeded the push for several new modified gravity (MG) theories, to understand our Universe without DM [38] or at least to connect the accelerated expansion to some new features of gravity [39].

A first drive for MG came from fundamental problems in the hot big bang model (horizon, flatness, and monopole problem solved within the inflationary paradigm [40,41]) and another one from galaxy rotation curves with solutions attempted within the modified Newtonian dynamics (MOND) [42] and the "modified gravity" (MOG) paradigm 43]] and $f(R)$ theories [44].

Alternative proposals to explain the accelerated expansion of the Universe increased exponentially. Besides

*Corresponding author.
adelpopolo@oact.inaf.it
†francesco.pace@manchester.ac.uk
‡d.f.mota@astro.uio.no

DM-like DE schemes [45–48], MG theories attempted to explain such acceleration as the manifestation of extra dimensions or higher-order corrections effects, as in the Dvali-Gabadadze-Porrati model [49] and in $f(R)$ gravity. Nowadays, the catalog of MG theories includes many theories, among which we recall $f(R)$ [44], $f(T)$ [50], MOND and BIMOND [42,51], tensor-vector-scalar theory [52], scalar-tensor-vector gravity theory (MOG) [43], Gauss-Bonnet models [53,54], Lovelock models [55], Hořava-Lifshitz [56], Galileons [57], and Horndeski [58,59]. The freedom allowed to MG from observations reduces to modifications on large scales (typically Hubble scales), low accelerations ($a_0 \lesssim 10^{-8}$ cm s^{-2}), or small curvatures (typically $R_\Lambda \simeq 1.2 \times 10^{-30}\, R_\odot$ [60]). Some theories violate Birkhoff's theorem, and this induces effects that should be disentangled wisely, as they make local tests complex. Such local tests, using PPN-like parameters[1] [61–64] and the GR condition on the two Newtonian potentials $\Phi = \Psi$, provide a smoking gun for MG, combining galaxy surveys ($\propto \Phi$), the integrated Sachs-Wolfe effect [65] in the CMB [$\propto \int dl(\dot{\Phi} + \dot{\Psi})$], and weak lensing [$\propto \int dl(\Phi + \Psi)$]. Real opportunities will come with future surveys: both from satellites (Euclid [66] and JDEM [67]) and ground-based (SKA [68] and LSST [69]). Another smoking gun should proceed from the best fitting of the CMB between DM and MG to constrain the parameters of the models [70,71].

For MG theories not to alter the behavior of gravity at small scales (e.g., Solar System) and reproduce the observational measurements [63,72], it is necessary to have some screening mechanism which hides undesired effects on small scales [73]. Following Ref. [74], we consider the case of the symmetron scalar-tensor theory [75] and the chameleon $f(R)$ gravity [76].

Effects of MG can be probed with structure formation and verified by means of dark-matter-only N-body simulations [77–81]. Nevertheless, hydrodynamical simulations are more suited from an observational point of view, as they provide observables, such as the halo profile, the turnaround [82,83], the splashback radius [84], and the mass-temperature relation (MTR) [74] which can be directly compared with observations. While the halo profile is usually studied in DM-only simulations and it is, as such, used for a variety of studies, the MTR can be accurately inferred only with hydrodynamic simulations, to avoid the necessary approximations introduced, for example, by using scaling relations. The MTR has been used to put constraints on MG theories. By means of hydrodynamic simulations, Ref. [74] showed that the MTR obtained in MG theories is different from the expectations of GR.[2]

In the present paper, we extended the results of Ref. [85] to take into account the effects of dynamical friction and the cosmological constant and revisited the results of Ref. [74] to show that the MTR is not a good probe to disentangle MG from GR. To this aim, we use a semianalytic model to show that in a ΛCDM model the MTR has a behavior similar to those obtained by Ref. [74], and this makes it impossible to disentangle between the MG results and those of GR.

The paper is organized as follows. Section II briefly presents the modified gravity models analyzed in this work, while Sec. III describes the model used to derive the MTR relation in ΛCDM cosmologies. Section IV is devoted to the presentation and the discussion of our results. We conclude in Sec. V.

In this work, we use the following cosmological parameters: $h_0 = 0.7$, $\Omega_\Lambda = 0.727$, $\Omega_{\rm DM} = 0.227$, and $\Omega_{\rm b} = 0.046$. An overbar will indicate quantities evaluated at the background level.

II. MODIFIED GRAVITY: MODELS AND SIMULATIONS

In this section, we summarize the modified gravity theories used by Ref. [74] that we compare our model to. These are scalar-tensor theories of gravity described by the action

$$S = \int \mathrm{d}^4x\sqrt{-g}\left[\frac{1}{2}M_{\rm pl}^2 R - \frac{1}{2}\partial^i\varphi\partial_i\varphi - V(\varphi)\right] + S_{\rm m}(\tilde{g}_{\mu\nu}, \varphi_i), \quad (1)$$

where g is the determinant of the metric tensor $g_{\mu\nu}$, R the Ricci scalar, $M_{\rm pl} = 1/\sqrt{8\pi G}$ the reduced Planck mass (in natural units where $\hbar = c = 1$), and φ and $V(\varphi)$ the scalar field and the self-interacting potential, respectively. Matter is described by the total matter action $S_{\rm m}$. The scalar field is conformally coupled to matter via $\tilde{g}_{\mu\nu} = A(\varphi)g_{\mu\nu}$, with $A(\varphi)$ the conformal factor.

The conformal coupling between matter and field gives rise to a fifth force of the form

[1]The parametrized post-Newtonian (PPN) formalism is a tool expressing Einstein's equations in terms of the lowest-order deviations from Newton's law of gravitation.

[2]In the literature, there is no explicit emphasis on what is exactly meant for mass. In general, when considering both numerical simulations and observations, the mass has to be the virial mass, as a result of the application of the virial theorem. This is more appropriately true for observations but less for N-body simulations, as the spherical overdensity procedure obtained to infer structures assumes a virial overdensity but does not automatically imply the virial theorem holding. Furthermore, the virial overdensity chosen will depend on which probe is considered (i.e., Sunyaev-Zel'dovich effect or x-ray emission); therefore, the virial mass will be interpreted differently in different scenarios. We therefore prefer to just call it mass, having in mind it is related to the true virial mass of the object.

$$F_\varphi = -\frac{A'(\varphi)}{A(\varphi)}\nabla\varphi, \tag{2}$$

where a prime indicates the derivative with respect to the scalar field.

A. Symmetron

The screening mechanism of the symmetron model [76] produces a strong coupling between matter and the extra field in low-density regions, while in high-density regions the scalar degree of freedom decouples from matter.

For this mechanism to work, one requires, around $\varphi = 0$, a coupling of the form

$$A(\varphi) = 1 + \frac{1}{2}\left(\frac{\varphi}{M}\right)^2 \tag{3}$$

and a potential

$$V(\varphi) = V_0 - \frac{1}{2}\mu^2\varphi^2 + \frac{1}{4}\lambda\varphi^4, \tag{4}$$

where M and μ are mass scales and λ a dimensionless parameter.

The free parameters can be recast in terms of the strength of the scalar field, β, the expansion factor at the symmetry breaking time, $a_{\rm SSB}$, and the range of the fifth force, λ_0. The fifth force then reads

$$F_\varphi = -\frac{\varphi}{M^2}\nabla\varphi = 6\Omega_{\rm m}H_0^2\frac{\beta^2\lambda_0^2}{a_{\rm SSB}^3}\tilde{\varphi}\nabla\tilde{\varphi}, \tag{5}$$

where the quantities with tilde are in the supercomoving coordinates [86].

B. $f(R)$ gravity

The $f(R)$-gravity models are theories in which the Ricci scalar in the Einstein-Hilbert action is substituted by a function of the same quantity, and it is described by the following action:

$$S = \frac{1}{2}M_{\rm pl}^2\int {\rm d}^4x\sqrt{-g}[R + f(R)]. \tag{6}$$

When $f(R) = -2\Lambda$, the ΛCDM model is recovered.

Typical of these theories is the chameleon screening mechanism, characterized by a local density dependence of the scalar field mass. In high-density environments, the scalar degree of freedom is very short ranged, and the opposite happens in low-density fields, where deviations from GR are maximized.

Reference [74] used the Hu-Sawicki [75] model, whose functional form is

$$f(R) = -m^2\frac{c_1(R/m^2)^n}{1 + c_2(R/m^2)^n}, \tag{7}$$

where the free parameter $m^2 = H_0^2\Omega_{\rm m,0}$ has dimensions of mass squared and $n > 0$. The two additional constants c_1 and c_2 can be determined by requiring that, in the large curvature regime ($R/m^2 \gg 1$), $f(R) \approx -2\Lambda$:

$$\frac{c_1}{c_2} \approx 6\frac{\Omega_{\Lambda,0}}{\Omega_{\rm m,0}}. \tag{8}$$

The strength of gravity modifications is encoded in the value of $f_R = df/dR$ today:

$$f_{R0} = -n\frac{c_1}{c_2^2}\left[\frac{\Omega_{\Lambda,0}}{3(\Omega_{\rm m,0} + 4\Omega_{\Lambda,0})}\right]^{n+1}. \tag{9}$$

The range of the scalar degree of freedom is $\lambda_0 \propto \sqrt{1/f_{R0}}$.

To derive the expression of the fifth force for $f(R)$ models, it is useful to transform them into scalar-tensor theories using the conformal transformation $A(\varphi) = \exp(-\beta\varphi/M_{\rm pl})$, where $\beta = \sqrt{6}/6$. We then find

$$F_\varphi = -\frac{a^2\beta}{M_{\rm pl}}\nabla\varphi, \tag{10}$$

with a the scale factor.

C. Simulations

In order to get the MTR for $f(R)$ and symmetron models, Ref. [74] modified the ISIS code [80] and ran two sets of simulations, one for $f(R)$-gravity models and another one for the symmetron models, both containing 256^3 DM particles. The box size and background cosmology were different for the two models, due to consistency with previous works of the authors [87]. In the case of the $f(R)$ gravity (symmetron), the DM particle mass was $3\times10^{10}\ M_\odot/h$ ($8.32\times10^{10}\,M_\odot/h$), $\Omega_\Lambda = 0.727$, $\Omega_{\rm CDM} = 0.227$, and $\Omega_{\rm b} = 0.045$ ($\Omega_\Lambda = 0.65$, $\Omega_{\rm CDM} = 0.3$, and $\Omega_{\rm b} = 0.05$), and the box size 200 Mpc h^{-1} (256 Mpc h^{-1}), with $h = 0.7$ ($h = 0.65$).

Because of the different parameters for $f(R)$ and symmetron models, the background ΛCDM model of the two models is different. Table 2 in Ref. [74] summarizes the parameters employed.

III. THE MODEL

In the next sections, we will discuss how the top-hat model (THM) can be improved and how the MTR is calculated. We show two different models, the "late-formation approximation" (see the following) and a model in which structures form continuously.

A. Improvements to the top-hat model

Using scaling arguments, one can show that there exists a relation between the x-ray mass of clusters and their temperature T_X. The mass in the virial radius can be written as $M(\Delta_{vir}) \propto T_X^{3/2}\rho_c^{-1/2}\Delta_{vir}^{-1/2}$, where ρ_c is the critical density and Δ_{vir} the density contrast of a spherical top-hat perturbation after collapse and virialization.

The previous relation shows a correlation between the mass and temperature, but this result can be highly improved. One possibility is to improve the THM, taking into account the angular momentum acquired by the interaction with neighboring protostructures, dynamical friction, and a modified version of the virial theorem, including a surface pressure term [88–91] due to the fact that at the virial radius r_{vir} the density is different from zero, as done in Ref. [92].

A further improvement can be obtained by taking into account that clusters form in a quasicontinuous way. To this aim, one substitutes the top-hat cluster formation model by a model of cluster formation from spherically symmetric perturbations with negative radial density gradients. The merging-halo formalism of Ref. [93] is used to take into account the gradual way clusters form.

To start with, we consider some gravitationally growing mass concentration collecting into a potential well. Let $dP = f(L, r, v_r, t)dLdv_rdr$ be the probability that a particle, having angular momentum $L = rv_\theta$, is located at $[r, r + dr]$, with velocity $(v_r = \dot{r})$ $[v_r, v_r + dv_r]$ and angular momentum $[L, L + dL]$. The term L takes into account ordered angular momentum generated by tidal torques and random angular momentum (see Appendix C.2 in Ref. [35]). The radial acceleration of the particle [92,94–97] is

$$\frac{dv_r}{dt} = -\frac{GM}{r^2} + \frac{L^2(r)}{M^2r^3} + \frac{\Lambda}{3}r - \eta\frac{dr}{dt}, \tag{11}$$

with Λ being the cosmological constant and η the dynamical friction coefficient. The previous equation can be obtained via Liouville's theorem [92]. The last term, the dynamical friction force per unit mass, is more explicitly given in Ref. [35] [Appendix D, Eq. (D5)]. A similar equation (excluding the dynamical friction term) was obtained by several authors (see, e.g., [98–100]) and generalized to smooth dark energy models in Ref. [101].

In the framework of general relativity, Refs. [102,103] derived the nonlinear evolution equation of the overdensity $\delta = \delta\rho_m/\bar{\rho}_m$ of nonrelativistic matter:

$$\ddot{\delta} + 2H\dot{\delta} - \frac{4}{3}\frac{\dot{\delta}^2}{1+\delta} - 4\pi G\bar{\rho}_m\delta(1+\delta) - (1+\delta)(\sigma^2 - \omega^2) = 0. \tag{12}$$

Recalling that $\delta = \frac{2GM_m}{\Omega_{m,0}H_0^2}(a/R)^3 - 1$, where R is the effective perturbation radius and a the scale factor, substituting into Eq. (12) one gets [101]

$$\ddot{R} = -\frac{GM_m}{R^2} - \frac{GM_{de}}{R^2}(1 + 3w_{de}) - \frac{\sigma^2 - \omega^2}{3}R, \tag{13}$$

where M_m and M_{de} are the matter mass content of the perturbation and the mass of the dark energy component, respectively. The previous equations can be generalized to account for the presence of dynamical friction using Eckart's formalism [104]. The standard Friedmann equation is now augmented with a fluid describing the contribution of the viscosity:

$$\left(\frac{\dot{a}}{a}\right)^2 = H^2 = \frac{8\pi G}{3}(\bar{\rho}_v + \bar{\rho}_m + \bar{\rho}_\Lambda), \tag{14}$$

where $\bar{\rho}_\Lambda$ is the energy density of the cosmological constant, $\bar{\rho}_m = \bar{\rho}_{m,0}a^{-3}$ the matter component, and $\dot{\bar{\rho}}_v + 3H\bar{\rho}_v = 3H^2\xi_0\bar{\rho}_v^\nu$ the viscous component, with ξ_0 the bulk viscosity coefficient. The bulk viscosity is expressed as $\xi = \xi_0\bar{\rho}_v^\nu$, where ν is a real constant.

Integrating Eq. (11) with respect to r, we have

$$\frac{1}{2}\left(\frac{dr}{dt}\right)^2 = \frac{GM}{r} + \int_0^r \frac{L^2}{M^2r^3}dr + \frac{\Lambda}{6}r^2 - \int_0^r \eta\frac{dr}{dt} + \epsilon. \tag{15}$$

The specific binding energy of the shell, ϵ, can be obtained from the turnaround condition $\frac{dr}{dt} = 0$.

One can obtain the MTR combining energy conservation, the virial theorem, using Eq. (15) and the connection between kinetic energy K and the temperature [90]:

$$\langle K\rangle = \frac{3\tilde{\beta}Mk_BT}{2\mu m_p}, \tag{16}$$

where $\mu = 0.59$ is the mean molecular weight, k_B is the Boltzmann constant, m_p is the proton mass, $\tilde{\beta} = \beta[1 + f(1/\beta - 1)\Omega_{b,0}/\Omega_{m,0}]$, $\Omega_{b,0}$ $(\Omega_{m,0})$ is the baryonic (total) matter density parameter today, f is the fraction of the baryonic matter in the hot gas, and the parameter $\beta = \frac{\mu m_p\sigma_v^2}{k_BT}$, σ_v being the ratio of the mass-weighted mean velocity dispersion of the dark matter particles.

Using the virial theorem, we have [92,96,105]

$$\langle K\rangle = \frac{3\tilde{\beta}Mk_BT}{2\mu m_p} = -\frac{1}{2}\langle U_G\rangle - \langle U_L\rangle + \langle U_\Lambda\rangle + \langle U_\eta\rangle. \tag{17}$$

The brackets indicate time average (see [95]). The four terms represent the energy related to the gravitational potential, the angular momentum, the cosmological constant, and the dynamical friction, respectively.

Equation (17) does not take into account the surface pressure term we spoke about, though. Assuming [90]

$$\langle K\rangle + \langle E\rangle = 3P_{\rm ext}V = -\nu U, \tag{18}$$

with V the volume of the outer boundary of the virialized region, $P_{\rm ext}$ the pressure on the boundary, ν a constant, and U the total potential (see [90]), Eq. (17) reads now

$$\langle K\rangle = (1+\nu)\left(-\frac{1}{2}\langle U_{\rm G}\rangle - \langle U_{\rm L}\rangle + \langle U_\Lambda\rangle + \langle U_\eta\rangle\right). \tag{19}$$

In other words, the averaged kinetic energy differs by a factor $1+\nu$ from before.

In order to estimate the effect of the boundary pressure on the virial theorem, we consider an isothermal velocity dispersion ($\sigma_{\rm 1D} = {\rm const}$), and then $P = \rho_{\rm vir}\sigma^2_{\rm 1D}$, for which we have [89]

$$\langle K\rangle = \frac{\bar\rho_{\rm m,vir}}{2\rho(r_{\rm vir}) - \bar\rho_{\rm m,vir}}\langle E\rangle, \tag{20}$$

where $\bar\rho$ is the mean density within the virial radius. If the local density is negligible at $r_{\rm vir}$, the confining pressure is zero and $\langle K\rangle = -\langle E\rangle$. For a Navarro-Frenk-White profile and a typical cluster value of the concentration parameter $c \simeq 5$, we have $|\langle K\rangle/\langle E\rangle| \simeq 2$. References [106,107] studied in detail the effect of the quoted boundary pressure, finding that it changes significantly the final object. More in detail, it is found that the virial temperature is affected (larger than a uniform sphere but smaller than a truncated singular approximation sphere) and the extrapolated linear overdensity contrast $\delta_{\rm c}$ is slightly smaller, implying an earlier collapse.

We now use energy conservation in the form (see [92,96])

$$\begin{aligned}\langle E\rangle &= \langle K\rangle + \langle U_{\rm G}\rangle + \langle U_\Lambda\rangle + \langle U_{\rm L}\rangle + \langle U_\eta\rangle \\ &= U_{\rm G,ta} + U_{\Lambda,{\rm ta}} + U_{\rm L,ta} + U_{\eta,{\rm ta}},\end{aligned} \tag{21}$$

where the subscript "ta" stands for turnaround.

Combining Eqs. (19) and (21), solving for $\langle K\rangle$, and recalling Eq. (16), we obtain

$$\begin{aligned}\frac{k_{\rm B}T}{\rm keV} &= 1.58(\nu+1)\frac{\mu}{\beta}\frac{1}{\psi\xi}\Omega^{1/3}_{\rm m,0}\left(\frac{M}{10^{15}\,M_\odot h^{-1}}\right)^{2/3}(1+z_{\rm ta}) \\ &\times\left[1+\left(\frac{32\pi}{3}\right)^{2/3}\psi\xi\bar\rho^{2/3}_{\rm m,ta}\frac{1}{H_0^2\Omega_{\rm m,0}M^{8/3}(1+z_{\rm ta})}\right. \\ &\times\int_0^{r_{\rm eff}}\frac{L^2}{r^3}{\rm d}r - \frac{2}{3}\frac{\Lambda}{\Omega_{\rm m,0}H_0^2(1+z_{\rm ta})^3}(\psi\xi)^3 \\ &\left.-\frac{2^{10/3}}{3^{2/3}}\pi^{2/3}\left(\frac{\psi\xi}{\Omega_{\rm m,0}H_0^2}\right)\left(\frac{\rho_{\rm m,0}}{M}\right)^{2/3}\frac{1}{1+z_{\rm ta}}\int\eta\frac{{\rm d}r}{{\rm d}t}{\rm d}r\right],\end{aligned} \tag{22}$$

where $r_{\rm eff} = \psi r_{\rm ta} = \psi\xi(\frac{2GM}{\Omega_{\rm m,0}H_0^2})^{1/3}$, $r_{\rm ta}$ is the radius at the turnaround epoch $z_{\rm ta}$, $\Omega_{\rm m,0} = \frac{8\pi G\bar\rho_{\rm m,0}}{3H_0^2}$, $M = 4\pi\bar\rho_{\rm m,0}x_1^3/3$, and $\xi = r_{\rm ta}/x_1$.

The product $\psi\xi$, using the definitions of ψ, ξ, and M can be written as [see also Eq. (26) and Ref. [108]]

$$\psi\xi = \frac{r_{\rm eff}}{r_{\rm ta}}\frac{r_{\rm ta}}{x_1} = \frac{r_{\rm eff}}{r_{\rm ta}}\left(\frac{\bar\rho_{\rm m,0}}{\rho_{\rm ta}}\right)^{1/3}(1+z_{\rm ta})^{-1}, \tag{23}$$

where $\rho_{\rm ta}$ is the average density inside the perturbation at the turnaround.

Equation (22) can be also equivalently written, by using the notation of Ref. [108], in terms of $r_{\rm vir}$:

$$\begin{aligned}\frac{k_{\rm B}T}{\rm keV} &= 0.94(\nu+1)\frac{\mu}{\beta}\left(\frac{r_{\rm ta}}{r_{\rm vir}}\right)\left(\frac{\rho_{\rm ta}}{\bar\rho_{\rm m,ta}}\right)^{1/3}\Omega^{1/3}_{\rm m,0} \\ &\times\left(\frac{M}{10^{15}\,M_\odot h^{-1}}\right)^{2/3}(1+z_{\rm ta}) \\ &\times\left[1+\frac{15r_{\rm vir}\bar\rho_{\rm m,ta}}{\pi^2H_0^2\Omega_{\rm m,0}\rho_{\rm ta}^3r_{\rm ta}^9(1+z_{\rm ta})}\int_0^{r_{\rm vir}}\frac{L^2{\rm d}r}{r^3}\right. \\ &-\frac{2}{3}\frac{\Lambda}{H_0^2\Omega_{m,0}}\left(\frac{r_{\rm vir}}{r_{\rm ta}}\right)^3\left(\frac{\bar\rho_{\rm m,ta}}{\rho_{\rm ta}}\right)\frac{1}{(1+z_{\rm ta})^3} \\ &\left.-\frac{6^{1/3}}{\pi^{1/3}}r_{\rm vir}r_{\rm ta}\left(\frac{\bar\rho_{\rm m,ta}}{\rho_{\rm ta}}\right)^{1/3}\left(\frac{\bar\rho_{\rm m,0}}{M}\right)^{2/3}\frac{1}{1+z_{\rm ta}}\frac{\lambda_0}{1-\mu(\delta)}\right],\end{aligned} \tag{24}$$

where $\Omega_\Lambda = \frac{\Lambda}{3H_0^2} = 1-\Omega_{\rm m,0}$. In Eq. (24), we integrated the term containing the dynamical friction; λ_0 and $\mu(\delta)$ are given in Ref. [109].

The value of $r_{\rm eff}$, as shown in Refs. [85,96], is given by the solution of the cubic equation:

$$\begin{aligned}&1-\nu+(\xi\psi)^3(\nu+2)\zeta - \psi(2+\zeta\xi^3) \\ &-\frac{27}{32}\frac{\xi^9\psi}{\rho_{\rm ta}^3\pi^3Gr_{\rm ta}^8}\left[\nu\int_0^{r_{\rm eff}}\frac{L^2}{r^3}{\rm d}r + \int_0^{r_{\rm ta}}\frac{L^2}{r^3}{\rm d}r\right. \\ &-\frac{16\pi^2}{9}(2+\nu)\rho_{\rm ta}^2r_{\rm ta}^6 \\ &\left.\times\left(\int_0^{r_{\rm eff}}\eta\frac{{\rm d}r}{{\rm d}t}{\rm d}r - \frac{1}{2+\nu}\int_0^{r_{\rm ta}}\eta\frac{{\rm d}r}{{\rm d}t}{\rm d}r\right)\right] = 0,\end{aligned} \tag{25}$$

where

$$\zeta = \frac{\Lambda}{4\pi G\rho_{\rm ta}} = \frac{\Lambda r_{\rm ta}^3}{3GM} = \frac{2\Omega_{\Lambda,0}}{\Omega_{m,0}}\frac{\bar\rho_{\rm m,ta}}{\rho_{\rm ta}}(1+z_{\rm ta})^{-3}. \tag{26}$$

The parameter ν, as shown by Ref. [90] [Eq. (47)], depends on the concentration parameter and the density profile. We fixed it as $\frac{\nu+1}{\nu-1} \simeq 2$ [89,90], for a typical value of the cluster concentration parameter, $c \simeq 5$.

B. Revisiting the continuous formation model

The approximation in which we found the MTR is known as the late-formation approximation and assumes

that perturbation clusters form from having a top-hat density profile and that the redshift of observation, $z_{\rm obs}$, is equal to that of formation, $z_{\rm f}$. The quoted approximation is good in the case $\Omega_{\rm m,0} \simeq 1$, where cluster formation is fast, and at all redshifts $z_{\rm obs} \simeq z_{\rm f}$. For the actual value of $\Omega_{\rm m,0}$, one needs to take into account the difference between $z_{\rm obs}$ and $z_{\rm f}$. Moreover, as shown by Ref. [89], continuous accretion is needed to get the correct normalization of the MTR and its time evolution.

In order to improve the THM, one can take into account the formation redshift [110,111] or the THM can be replaced by a model in which clusters form from spherically symmetric perturbations [88,89], combined with the merging-halo formalism of Ref. [93]. In this way, one moves from a model in which clusters form instantaneously to one in which they form gradually.

Integrating Eq. (15), one gets

$$t = \int \frac{{\rm d}r}{\sqrt{2[\epsilon + \frac{GM}{r} + \int_{r_{\rm i}}^{r} \frac{L^2}{M^2 r^3}{\rm d}r + \frac{\Lambda}{6} r^2] - \int \eta \frac{{\rm d}r}{{\rm d}t}{\rm d}r}}. \quad (27)$$

Following Ref. [89], we may write the specific energy of infalling matter as

$$\epsilon_l = -\frac{1}{2}\left(\frac{2\pi G M}{t_\Omega}\right)^{2/3}\left[\left(\frac{M_0}{M}\right)^{5/(3m)} - 1\right] g(M), \quad (28)$$

where $t_\Omega = \pi\Omega_{\rm m,0}/[H_0(1-\Omega_{\rm m,0})^{3/2}]$, M_0 is a fiducial mass, m is a constant specifying how the mass variance evolves as a function of M, and the function $g(M)$ reads

$$g(M) = 1 + \frac{F}{x-1} + \frac{\lambda_0}{1-\mu(\delta)} + \frac{\Lambda}{3H_0^2\Omega_{\rm m,0}}\xi^3, \quad (29)$$

where $x = 1 + (t_\Omega/t)^{2/3}$ is connected to the mass by $M = M_0 x^{-3m/5}$, M_0 is given in Ref. [89], and

$$F = \frac{2^{7/3}\pi^{2/3}\bar{\rho}_{\rm m,0}^{2/3}}{3^{2/3}H_0^2\Omega_{\rm m,0}M^{8/3}}\int_{r_{\rm i}}^{r_{r_{\rm ta}}} \frac{L^2}{r^3}{\rm d}r. \quad (30)$$

In order to calculate the kinetic energy E, we integrate ϵ_l with respect to the mass [89] to get $-\int \epsilon_l dM = E/M$. Finally, we have

$$k_{\rm B}T = \frac{4}{3}\tilde{a}\frac{\mu m_{\rm p}}{2\beta}\frac{E}{M}, \quad (31)$$

where $\tilde{a} = \frac{\bar{\rho}_{\rm m,vir}}{2\rho(r_{\rm vir}) - \bar{\rho}_{\rm m,vir}}$ is the ratio between kinetic and total energy [89] and $\bar{\rho}_{\rm m,vir}$ the mean density within the virial radius. Calculating E/M, we obtain

$$\frac{k_{\rm B}T}{\rm keV} = \frac{2}{5}\tilde{a}\frac{\mu m_{\rm p}}{2\beta}\frac{m}{m-1}\left(\frac{2\pi G}{t_\Omega}\right)^{2/3} M^{2/3} \times \left[\frac{1}{m} + \left(\frac{t_\Omega}{t}\right)^{2/3} + \frac{K(m,x)}{(M/M_0)^{8/3}} + \frac{\lambda_0}{1-\mu(\delta)} + \frac{\Lambda\xi^3}{3H_0^2\Omega_{\rm m,0}}\right], \quad (32)$$

where

$$K(m,x) = (m-1)Fx\,{\rm LerchPhi}(x,1,3m/5+1) - (m-1)F\,{\rm LerchPhi}(x,1,3m/5), \quad (33)$$

and LerchPhi is a function defined as follows[3]:

$${\rm LerchPhi}(z,a,v) = \sum_{n=0}^{\infty}\frac{z^n}{(v+n)^a}. \quad (34)$$

Following Ref. [89] to get the normalization, Eq. (32) can be written as [92]

$$k_{\rm B}T \simeq 8\ {\rm keV}\left(\frac{M}{10^{15}\ h^{-1}\,M_\odot}\right)^{2/3}\frac{m(M)}{n(M)}. \quad (35)$$

The functions $m(M)$ and $n(M)$ are defined as

$$m(M) = \frac{1}{m} + \left(\frac{t_\Omega}{t}\right)^{2/3} + \frac{K(m,x)}{(M/M_0)^{8/3}} + \frac{\lambda_0}{1-\mu(\delta)} + \frac{\Lambda\xi^3}{3H_0^2\Omega_{\rm m,0}}, \quad (36)$$

$$n(M) = \frac{1}{m} + \left(\frac{t_\Omega}{t_0}\right)^{2/3} + K_0(m,x), \quad (37)$$

where $K_0(m,x)$ indicates that $K(m,x)$ must be calculated assuming $t = t_0$.

When compared to Eq. (17) of Ref. [89], Eq. (35) shows an additional mass-dependent term. This means that, as in the case of the top-hat model, the MTR is no longer self-similar, showing a break at the low-mass end (see the next section).

Besides Refs. [88,89], Ref. [90] found a MTR and its scatter. Their result concerning the MTR and the scatter is in agreement with the result we found here. In this case,

$$k_{\rm B}T = 6.62\ {\rm keV}\,Q\left(\frac{M}{10^{15}\ h^{-1}\,M_\odot}\right)^{2/3}, \quad (38)$$

where

[3]This definition is valid for $|z| < 1$. By analytic continuation, it is extended to the whole complex z plane for each value of a.

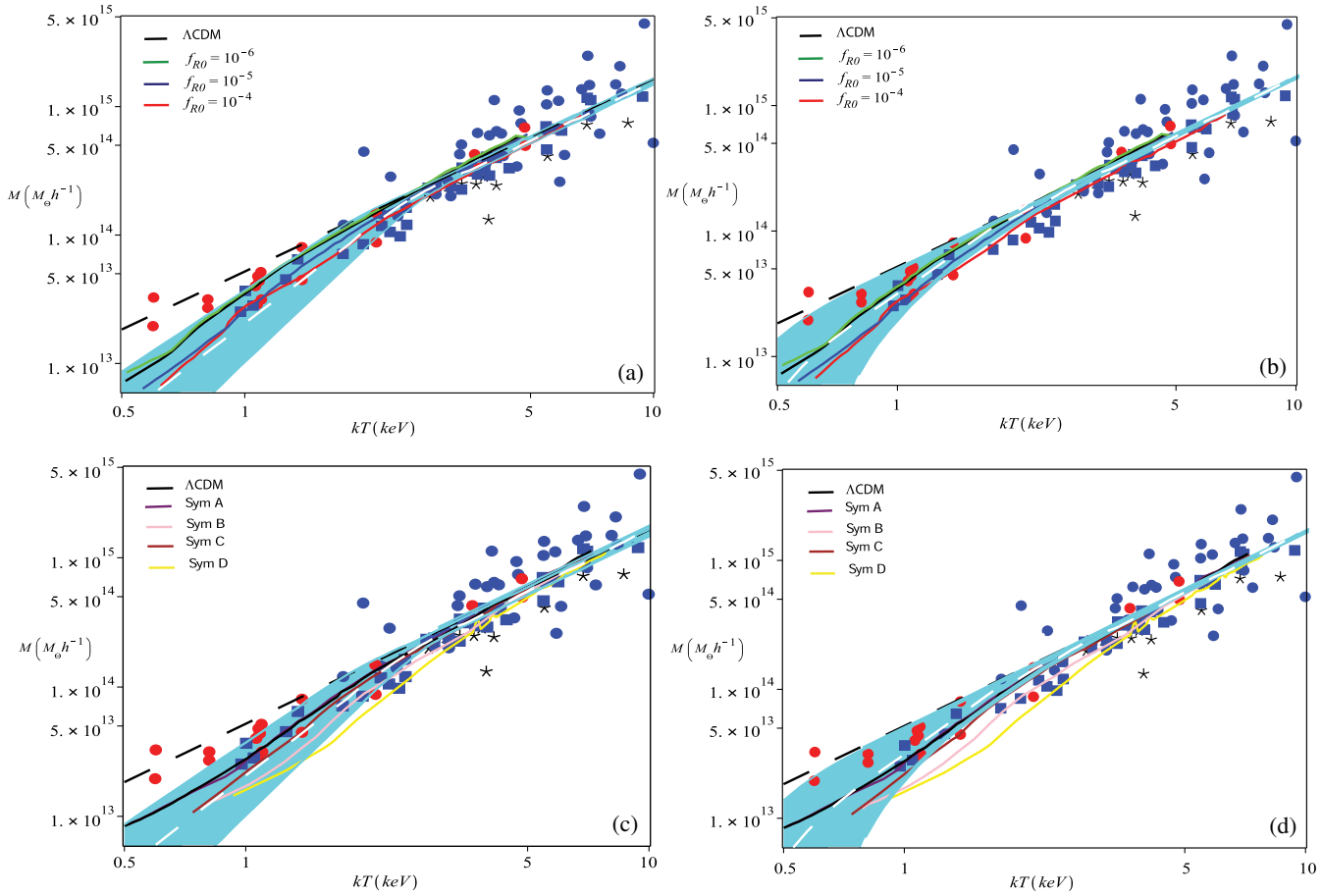

FIG. 1. The MTR for $f(R)$ (top panels) and symmetron models (bottom panels). In all the panels, the black line shows the ΛCDM model, and the dashed black line shows the MTR $\propto T^{3/2}$ as obtained from scaling relations, while the stacked galaxy clusters are depicted with red and blue circles, blue squares, and black stars. In (a) (top left) and in (b) (top right), the cyan region shows the 68% confidence level region, obtained using the continuous formation model [Eq. (35)] and the model by Ref. [90] [Eq. (39)], respectively. The white dashed line is the average value. The red, blue, and green lines represent the $f(R)$ model with three different normalizations. (c) (bottom left) and (d) (bottom right) are the equivalent of (a) and (b) for the symmetron models.

$$Q = \frac{1+\nu}{1-\nu}\frac{B}{A(Ht)^{2/3}} \tag{39}$$

and where B/A is a constant [see the discussion after Eq. (25) in Ref. [90]] and ν was defined in Eq. (18).

IV. RESULTS AND DISCUSSION

In Fig. 1, we show the results of the comparison between our continuous formation model [Eq. (35)] and the model by Ref. [90] with that of Ref. [74] for $f(R)$ and symmetron models. For $f(R)$ models, we consider $n = 1$ and $|f_{R0}| = 10^{-4}, 10^{-5}, 10^{-6}$, while for the symmetron model $(\beta, a_{\rm SSB}, \lambda_0) = (1.0, 0.5, 1.0)$ for Sym A, (1.0, 0.33, 1.0) for Sym B, (2.0, 0.5, 1.0) for Sym C, and (1.0, 0.25, 1.0) for Sym D.

In all the panels, the black straight dashed line represents the classical MTR self-similar behavior and the black solid line the ΛCDM model obtained in the simulations of Ref. [74], and for the specific modified gravity models we refer to the caption of Fig. 1. Observational data are represented by points. Red circles come from Ref. [112], while blue points are from Ref. [113]. Stars are from Ref. [113] and represent data using spatially resolved observations.

Figure 1(a) (top left panel) compares the result of our continuous formation model for the $f(R)$ models presented in Ref. [74] (HM). The cyan band represents the 68% confidence level region, obtained using the continuous formation model [Eq. (35)] and calculated similarly to Ref. [90] (Sec. 3.7). The white dashed line is the average value. As expected, deviations from the ΛCDM model are larger for the model with $f_{R0} = -10^{-4}$, as it represents the model with the strongest modifications to gravity. For smaller values of f_{R0}, at temperatures $T < 1$ keV, data are in partial agreement with both the $f(R)$ cosmology and the model presented in this work.

Data points have a large dispersion and circumscribe the theoretical models at high mass, while at the lowest masses data have a value larger than the simulated HM models and the result of our model. Stars show lower masses than the models considered. At high mass, all models are indistinguishable, while at small masses differences become visible.

This is because effects of modified gravity depend on the environment and, hence, on the density. In high-density regions, screening takes place and deviations from ΛCDM are smaller. Therefore, in high-density regions the ΛCDM MTR has a similar behavior to that of modified gravity models.

Our model shows a non-self-similar behavior and presents a break at $T \simeq 3$ keV. At small masses, the slope of the central (average) curve, in the range 0.5–3 keV, is $\simeq 2.3$, and the cyan region has an inner and outer slope of 1.8 and 3, respectively. The quoted bend has been observed in the literature by several authors (see, e.g., [114]), who, assuming the cluster temperature to be constant after the formation time, explained the break as due to the formation redshift. Another possibility is that the cluster medium is preheated in the early phase of formation [115]. Reference [90], instead, justified the break with the scatter in the density field. The result of the model of Ref. [90] is shown in Fig. 1(b) (top right panel), where once again the cyan region represents the 68% confidence level region (see Ref. [90], Sec. 3.7).

This model is not able to distinguish between the effect of formation redshift from scatter in the initial energy of the cluster or its initial nonsphericity. However, the presence of nonsphericity gives rise to a mass-dependent asymmetric scatter in the MTR. This scatter is larger than that of the density field and at small temperatures covers all clusters except one, while the bend in the curve of Ref. [90] takes place almost at the same temperature, $T_X \simeq 3$ keV, in our model.

In our model, the bend is due to tidal interactions with neighboring clusters, arising from the asphericity of clusters (see [92] for a discussion on the relation between angular momentum acquisition, asphericity, and structure formation), and to the effect of dynamical friction. Asphericity gives rise to a mass-dependent asymmetric bend in the MTR. The lower the mass, the larger the difference from the classical self-similar solution. The origin of the bend is due to a few reasons. Our MTR, differently from others (e.g., [89,90]), contains a mass-dependent angular momentum, L, originating from the quadrupole moment of the protocluster with the tidal field of the neighboring objects. The presence of this additive mass-dependent term breaks the self-similarity of the MTR. To be more precise, the collapse in our model is different from the THM: The turnaround epoch and collapse time change, as well as the collapse threshold δ_c, which is now mass dependent and a monotonic decreasing function of the mass (see Fig. 1 in Ref. [116]). It is larger than the standard value at galactic masses and tends to the standard value when we move to the largest clusters. The temperature is $T \propto \epsilon \propto \delta_c$ (see [89]), and then less massive clusters are hotter than more massive ones, which are characterized by a standard MTR.

Besides the effect of angular momentum in changing the shape of the MTR, we must recall that another factor contributing is the modification of the partition of energy in virial equilibrium, which influences the shape of the MT relation. At the same time, an important role is played by the cosmological constant and dynamical friction. Both effects, similarly to that of angular momentum, delay the collapse of the perturbation. A comparison of the three effects, the three terms in Eq. (11), are shown in Fig. 1 of Ref. [116] and in Fig. 11 of Ref. [35]. They are all of the same order of magnitude with differences of a few percent. The effect of dynamical friction (DF) was calculated as shown in Refs. [35,117,118].

The first calculations of the role of DF in clusters formation is due to Refs. [119–122], who considered the DF generated by the galactic population on the motion of galaxies themselves. Reference [117] took into account also the effects of substructure and showed DF produces a collapse delay in the collapse of low-ν peaks, with several consequences, like the mass accumulated by the peak, and similarly to tidal torques.

As a consequence of dynamical friction and tidal torques, one expects changes in the threshold of collapse, the temperature at a given mass (since $T \propto \delta_c$), the mass function, and the correlation function. DF and angular momentum have similar effects on structure formation: They delay the collapse and have similar consequences on the collapse threshold.

An important result of the previous calculation is that the MTR in modified gravity cannot be distinguished from that predicted by the ΛCDM model. In HM, the MTR in modified gravity was very different from that of ΛCDM prediction for colder clusters and indistinguishable for hotter ones. Our plots show that the MTR bends in a similar way as done by the MTR in the $f(R)$ models and symmetron models (see the following). The bending was explained previously and is related to the effect of several factors as the acquisition of angular momentum through tidal torques, by dynamical friction, and by the cosmological constant.

Our model and the $f(R)$ and symmetron models (see the following) of Ref. [74] are in agreement with data till $\simeq 1$ keV; at lower temperatures, a discrepancy is observed with the few clusters present. A similar result is found comparing the $f(R)$ models with the model by Ref. [90], in Fig. 1(b). In this case, while $f(R)$ models are in disagreement with the data at small masses, this is no longer true for the model by Ref. [90] and ΛCDM. However, there is a slight disagreement between the model with $f_{R0} = -10^{-4}$ and Ref. [90].

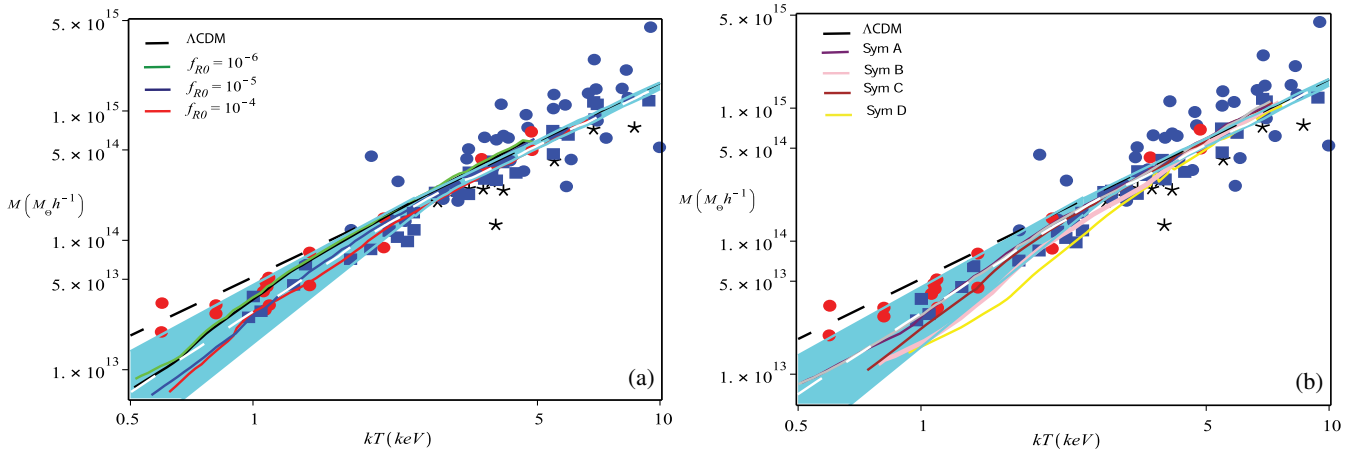

FIG. 2. The MTR for $f(R)$ (left panel) and symmetron models (right panel). Lines and symbols represent the same quantities as in Fig. 1, but now the cyan region is the 68% confidence level region, obtained by means of the improved top-hat model [Eq. (24)].

In particular, in the case of the $f(R)$ models, Figs. 1(a) and 1(b) show that our model is in agreement with all $f(R)$ models considered. In Fig. 1(b), the slope of the average value, in the range 0.5–3 keV, is $\simeq 2.3$, while that of the inner cyan region $\simeq 1.8$ and that of the outer cyan region > 3 for temperatures < 1 keV.

Figure 1(c) shows the same quantities plotted in Figs. 1(a) and 1(b) but for the symmetron case. The plot shows that model Sym D is the one which deviates the most from the ΛCDM, followed by Sym C, Sym B, and Sym A. Again, at high mass, till $\simeq 4$ keV, our model, the symmetron models, and the data are indistinguishable, but Sym D, even if in agreement with the data till $\simeq 3$ keV, slightly differs from our model, namely, with the ΛCDM predictions. The discrepancy goes on till $\simeq 2$ keV and then disappears. All the other symmetron models are in agreement with our model. As in Fig. 1(a), for $T \leq 1$ keV, the models are in disagreement with a few clusters. Notice that in Figs. 1(a) and 1(c), we compare the continuous formation model with the $f(R)$ and symmetron model, respectively, and then the only change between the two plots is due to the $f(R)$ and symmetron curves. The slopes are then the same as in Fig. 1(a).

Finally, in Fig. 1(d), we show the same results as in Fig. 1(c) but for the model by Ref. [90]. The result is similar to Fig. 1(b). In this case, in the range $1 \leq T/\text{keV} \leq 4$, the model by Ref. [90] differs from Sym B and D.

The larger discrepancy between the model by Ref. [90] and the symmetron models in the temperature range 1–4 keV with respect to the predictions of our model is probably due to the fact that, as stressed by Ref. [90], the calculation of the effects of the nonspherical shape of the initial protocluster are not very rigorous and should be considered as an estimate of the actual corrections. The previous assertion is somehow confirmed by the fact that in the given range there is not a real discrepancy between cluster data and the other models (except with the model by Ref. [90]).

We want to stress that the quoted discrepancies between ΛCDM predictions and Sym B and D, however, do not imply that the symmetron model can be used to claim the MTR is a probe to distinguish between modified gravity and ΛCDM, since in the quoted temperature range there are no visible peculiar differences between the cluster data and the model.

As before, we stress that Figs. 1(d) and 1(b) differ only for the curves relative to the $f(R)$ and symmetron models, since we are comparing the last with the same model, namely, Ref. [90] [Eq. (39)]. The slopes are then the same as in Fig. 1(b).

Finally in Figs. 2(a) and 2(b), we compare the results of the improved top-hat model [Eq. (24)] with the $f(R)$ [Fig. 2(a)] and the symmetron models [Fig. 2(b)] of Ref. [74]. The results are similar to those plotted in Figs. 1(a) and 1(c), with the difference that the slope discussed previously is now smaller. The differences between the model plotted in Figs. 1(a) and 1(c) (revised top hat) and that in Figs. 2(a) and 2(b) (continuous formation model) are due to the assumed redshift of formation in the two models. The slope of the average curve is $\simeq 2$, and those of the outer and inner cyan region $\simeq 1.8$ and $\simeq 2.5$, respectively.

Before concluding, we want to add a note on the redshift dependence of the observed cluster data and the MTR which depends on the redshift. All the quantities involved in the determination are, formally, time dependent (concentration and temperature). Therefore, when evaluating the MTR, one has to be cautious and aware of this, as the time evolution can have a substantial effect on the final result. Nevertheless, in our discussion, redshift evolution is not a concern as all the objects considered in Refs. [112,113] are nearby ($z \lesssim 0.2$), and neglecting it has a very small impact when compared to the observational error bars on the mass and temperature.

V. CONCLUSIONS

In the present work, we derived the MTR relationship using an improved top-hat model and a continuous formation model and compared the results with the prediction of Ref. [74] using $f(R)$ and symmetron models. Our model takes into account dynamical friction, the angular momentum acquired through tidal-torque interaction between clusters, and a modified version of the virial theorem including an external pressure. The continuous formation model is based on the merging-halo formalism by Ref. [93]. Both models give a MTR different from the classical self-similar behavior, with a break at 3–4 keV, and a steepening with a decreasing cluster temperature. The comparison of the quoted MTR with those obtained by Ref. [74] for $f(R)$ gravity and symmetron models shows that the MTR is not a good probe to test gravity theories, since the MTR for the ΛCDM model has the same behavior of that obtained by Ref. [74] for the two modified gravity theories considered.

ACKNOWLEDGMENTS

We thank an anonymous referee whose comments helped us to improve the quality of this work. D. F. M. thanks the Research Council of Norway for their support and the resources provided by UNINETT Sigma2—the National Infrastructure for High Performance Computing and Data Storage in Norway. This paper is based upon work from the COST action CA15117 (CANTATA), supported by COST (European Cooperation in Science and Technology). F. P. acknowledges support from STFC Grant No. ST/P000649/1.

[1] P. Bull *et al.*, Phys. Dark Universe **12**, 56 (2016).
[2] A. Del Popolo, Int. J. Mod. Phys. D **23**, 1430005 (2014).
[3] G. Bertone, D. Hooper, and J. Silk, Phys. Rep. **405**, 279 (2005).
[4] E. S. Battistelli, C. Burigana, P. de Bernardis, A. A. Kirillov, G. B. L. Neto, S. Masi, H. U. Norgaard-Nielsen, P. Ostermann, M. Roman, P. Rosati, and M. Rossetti, Int. J. Mod. Phys. D **25**, 1630023 (2016).
[5] F. R. Bouchet, Astrophys. Space Sci. **290**, 69 (2004).
[6] M. Kilbinger, Rep. Prog. Phys. **78**, 086901 (2015).
[7] A. Del Popolo, Astronomy Reports **51**, 169 (2007).
[8] J. Einasto, Astron. Soc. Pac. Conf. Ser. **252**, 85 (2001).
[9] M. Klasen, M. Pohl, and G. Sigl, Prog. Part. Nucl. Phys. **85**, 1 (2015).
[10] A. G. Riess, A. V. Filippenko, P. Challis *et al.*, Astron. J. **116**, 1009 (1998).
[11] A. V. Astashenok and A. del Popolo, Classical Quantum Gravity **29**, 085014 (2012).
[12] H. E. S. Velten, R. F. vom Marttens, and W. Zimdahl, Eur. Phys. J. C **74**, 3160 (2014).
[13] S. Weinberg, Rev. Mod. Phys. **61**, 1 (1989).
[14] D. N. Spergel, L. Verde, H. V. Peiris, E. Komatsu, M. R. Nolta, C. L. Bennett, M. Halpern, G. Hinshaw, N. Jarosik, A. Kogut, M. Limon, S. S. Meyer, L. Page, G. S. Tucker, J. L. Weiland, E. Wollack, and E. L. Wright, Astrophys. J. Suppl. Ser. **148**, 175 (2003).
[15] E. Komatsu, K. M. Smith, J. Dunkley *et al.*, Astrophys. J. Suppl. Ser. **192**, 18 (2011).
[16] B. Moore, T. Quinn, F. Governato, J. Stadel, and G. Lake, Mon. Not. R. Astron. Soc. **310**, 1147 (1999).
[17] W. J. G. de Blok, Adv. Astron. **2010**, 789293 (2010).
[18] J. P. Ostriker and P. Steinhardt, Science **300**, 1909 (2003).
[19] M. Boylan-Kolchin, J. S. Bullock, and M. Kaplinghat, Mon. Not. R. Astron. Soc. **415**, L40 (2011).
[20] A. Del Popolo and N. Hiotelis, J. Cosmol. Astropart. Phys. 01 (2014) 047.
[21] A. Del Popolo and M. Le Delliou, J. Cosmol. Astropart. Phys. 12 (2014) 051.
[22] A. Del Popolo and M. Le Delliou, Galaxies **5**, 17 (2017).
[23] H. K. Eriksen, F. K. Hansen, A. J. Banday, K. M. Górski, and P. B. Lilje, Astrophys. J. **605**, 14 (2004).
[24] D. J. Schwarz, G. D. Starkman, D. Huterer, and C. J. Copi, Phys. Rev. Lett. **93**, 221301 (2004).
[25] M. Cruz, E. Martínez-González, P. Vielva, and L. Cayón, Mon. Not. R. Astron. Soc. **356**, 29 (2005).
[26] C. J. Copi, D. Huterer, D. J. Schwarz, and G. D. Starkman, Mon. Not. R. Astron. Soc. **367**, 79 (2006).
[27] E. Macaulay, I. K. Wehus, and H. K. Eriksen, Phys. Rev. Lett. **111**, 161301 (2013).
[28] Planck Collaboration XVI, Astron. Astrophys. **571**, A16 (2014).
[29] M. Raveri, Phys. Rev. D **93**, 043522 (2016).
[30] A. R. Zentner and J. S. Bullock, Astrophys. J. **598**, 49 (2003).
[31] A. M. Brooks, M. Kuhlen, A. Zolotov, and D. Hooper, Astrophys. J. **765**, 22 (2013).
[32] J. Oñorbe, M. Boylan-Kolchin, J. S. Bullock, P. F. Hopkins, D. Kerěs, C.-A. Faucher-Giguère, E. Quataert, and N. Murray, Mon. Not. R. Astron. Soc. **454**, 2092 (2015).
[33] A. El-Zant, I. Shlosman, and Y. Hoffman, Astrophys. J. **560**, 636 (2001).
[34] A. A. El-Zant, Y. Hoffman, J. Primack, F. Combes, and I. Shlosman, Astrophys. J. Lett. **607**, L75 (2004).
[35] A. Del Popolo, Astrophys. J. **698**, 2093 (2009).
[36] C. Nipoti and J. Binney, Mon. Not. R. Astron. Soc. **446**, 1820 (2015).
[37] A. Del Popolo and F. Pace, Astrophys. Space Sci. **361**, 162 (2016).
[38] J. D. Bekenstein, Modified gravity as an alternative to dark matter, in *Particle Dark Matter: Observations, Models and Searches*, edited by G. Bertone (Cambridge University Press, Cambridge, England, 2010), p. 99.

[39] A. Joyce, L. Lombriser, and F. Schmidt, Annu. Rev. Nucl. Part. Sci. **66**, 95 (2016).
[40] A. A. Starobinskiĭ, Sov. J. Exp. Theor. Phys. Lett. **30**, 682 (1979).
[41] A. H. Guth, Phys. Rev. D **23**, 347 (1981).
[42] M. Milgrom, Astrophys. J. **270**, 365 (1983).
[43] J. W. Moffat, J. Cosmol. Astropart. Phys. 03 (2006) 004.
[44] A. De Felice and S. Tsujikawa, Living Rev. Relativity **13**, 3 (2010).
[45] C. Armendariz-Picon, V. Mukhanov, and P. J. Steinhardt, Phys. Rev. D **63**, 103510 (2001).
[46] A. Kamenshchik, U. Moschella, and V. Pasquier, Phys. Lett. B **511**, 265 (2001).
[47] R. de Putter and E. V. Linder, Astropart. Phys. **28**, 263 (2007).
[48] R. Durrer, *The Cosmic Microwave Background*, edited by R. Durrer (Cambridge University Press, England, 2008).
[49] G. Dvali, G. Gabadadze, and M. Porrati, Phys. Lett. B **485**, 208 (2000).
[50] E. V. Linder, Phys. Rev. D **81**, 127301 (2010).
[51] M. Milgrom, Phys. Rev. D **89**, 024027 (2014).
[52] J. D. Bekenstein, Phys. Rev. D **70**, 083509 (2004).
[53] B. Zwiebach, Phys. Lett. B **156**, 315 (1985).
[54] S. Nojiri, S. D. Odintsov, and M. Sasaki, Phys. Rev. D **71**, 123509 (2005).
[55] D. Lovelock, J. Math. Phys. (N.Y.) **12**, 498 (1971).
[56] P. Hořava, Phys. Rev. D **79**, 084008 (2009).
[57] Y. Rodríguez and A. A. Navarro, J. Phys. Conf. Ser. **831**, 012004 (2017).
[58] G. W. Horndeski, Int. J. Theor. Phys. **10**, 363 (1974).
[59] C. Deffayet, O. Pujolàs, I. Sawicki, and A. Vikman, J. Cosmol. Astropart. Phys. 10 (2010) 026.
[60] I. Debono and G. F. Smoot, Universe **2**, 23 (2016).
[61] W.-T. Ni, Astrophys. J. **176**, 769 (1972).
[62] C. M. Will, *Theory and Experiment in Gravitational Physics*, edited by C. M. Will (Cambridge University Press, Cambridge, England, 1993), p. 396.
[63] B. Bertotti, L. Iess, and P. Tortora, Nature (London) **425**, 374 (2003).
[64] C. M. Will, Living Rev. Relativity **17**, 4 (2014).
[65] F.-X. Dupé, A. Rassat, J.-L. Starck, and M. J. Fadili, Astron. Astrophys. **534**, A51 (2011).
[66] http://www.euclid-ec.org.
[67] http://jdem.lbl.gov/.
[68] https://www.skatelescope.org.
[69] https://www.lsst.org.
[70] R. A. Battye, B. Bolliet, and F. Pace, Phys. Rev. D **97**, 104070 (2018).
[71] D. Trinh, F. Pace, R. A. Battye, and B. Bolliet, Phys. Rev. D **99**, 043515 (2019).
[72] S. Dimopoulos, P. W. Graham, J. M. Hogan, and M. A. Kasevich, Phys. Rev. Lett. **98**, 111102 (2007).
[73] P. Brax, A.-C. Davis, B. Li, and H. A. Winther, Phys. Rev. D **86**, 044015 (2012).
[74] A. Hammami and D. F. Mota, Astron. Astrophys. **598**, A132 (2017).
[75] W. Hu and I. Sawicki, Phys. Rev. D **76**, 064004 (2007).
[76] K. Hinterbichler and J. Khoury, Phys. Rev. Lett. **104**, 231301 (2010).
[77] C. Llinares, A. Knebe, and H. Zhao, Mon. Not. R. Astron. Soc. **391**, 1778 (2008).
[78] G.-B. Zhao, B. Li, and K. Koyama, Phys. Rev. D **83**, 044007 (2011).
[79] E. Puchwein, M. Baldi, and V. Springel, Mon. Not. R. Astron. Soc. **436**, 348 (2013).
[80] C. Llinares, D. F. Mota, and H. A. Winther, Astron. Astrophys. **562**, A78 (2014).
[81] M. B. Gronke, C. Llinares, and D. F. Mota, Astron. Astrophys. **562**, A9 (2014).
[82] S. Bhattacharya, K. F. Dialektopoulos, A. Enea Romano, C. Skordis, and T. N. Tomaras, J. Cosmol. Astropart. Phys. 07 (2017) 018.
[83] R. C. C. Lopes, R. Voivodic, L. R. Abramo, and L. Sodré, Jr., J. Cosmol. Astropart. Phys. 09 (2018) 010.
[84] S. Adhikari, J. Sakstein, B. Jain, N. Dalal, and B. Li, J. Cosmol. Astropart. Phys. 11 (2018) 033.
[85] A. Del Popolo, Astron. Astrophys. **387**, 759 (2002).
[86] H. Martel and P. R. Shapiro, Mon. Not. R. Astron. Soc. **297**, 467 (1998).
[87] A. Hammami and D. F. Mota, Astron. Astrophys. **584**, A57 (2015).
[88] G. M. Voit and M. Donahue, Astrophys. J. Lett. **500**, L111 (1998).
[89] G. M. Voit, Astrophys. J. **543**, 113 (2000).
[90] N. Afshordi and R. Cen, Astrophys. J. **564**, 669 (2002).
[91] A. Del Popolo, N. Hiotelis, and J. Peñarrubia, Astrophys. J. **628**, 76 (2005).
[92] A. Del Popolo and M. Gambera, Astron. Astrophys. **344**, 17 (1999).
[93] C. Lacey and S. Cole, Mon. Not. R. Astron. Soc. **262**, 627 (1993).
[94] P. J. E. Peebles, *Principles of Physical Cosmology*, Princeton Series in Physics, edited by P. J. E. Peebles (Princeton University Press, Princeton, NJ, 1993).
[95] J. G. Bartlett and J. Silk, Astrophys. J. Lett. **407**, L45 (1993).
[96] O. Lahav, P. B. Lilje, J. R. Primack, and M. J. Rees, Mon. Not. R. Astron. Soc. **251**, 128 (1991).
[97] A. Del Popolo and M. Gambera, Astron. Astrophys. **337**, 96 (1998).
[98] P. Fosalba and E. Gaztañaga, Mon. Not. R. Astron. Soc. **301**, 503 (1998).
[99] S. Engineer, N. Kanekar, and T. Padmanabhan, Mon. Not. R. Astron. Soc. **314**, 279 (2000).
[100] A. Del Popolo, F. Pace, and J. A. S. Lima, Mon. Not. R. Astron. Soc. **430**, 628 (2013).
[101] F. Pace, C. Schimd, D. F. Mota, and A. Del Popolo, arXiv:1811.12105.
[102] F. Pace, J.-C. Waizmann, and M. Bartelmann, Mon. Not. R. Astron. Soc. **406**, 1865 (2010).
[103] F. Pace, S. Meyer, and M. Bartelmann, J. Cosmol. Astropart. Phys. 10 (2017) 040.
[104] C. M. S. Barbosa, J. C. Fabris, O. F. Piattella, H. E. S. Velten, and W. Zimdahl, arXiv:1512.00921.
[105] L. D. Landau and E. M. Lifshitz, *Lehrbuch der theoretischen Physik*, 4th ed. (Akademie-Verlag, Berlin, 1966).
[106] P. R. Shapiro, I. T. Iliev, and A. C. Raga, Mon. Not. R. Astron. Soc. **307**, 203 (1999).

[107] I. T. Iliev and P. R. Shapiro, Mon. Not. R. Astron. Soc. **325**, 468 (2001).
[108] P. B. Lilje, Astrophys. J. Lett. **386**, L33 (1992).
[109] S. Colafrancesco, V. Antonuccio-Delogu, and A. Del Popolo, Astrophys. J. **455**, 32 (1995).
[110] T. Kitayama and Y. Suto, Astrophys. J. **469**, 480 (1996).
[111] P. T. P. Viana and A. R. Liddle, Mon. Not. R. Astron. Soc. **281**, 323 (1996).
[112] X. Dai, C. S. Kochanek, and N. D. Morgan, Astrophys. J. **658**, 917 (2007).
[113] D. J. Horner, R. F. Mushotzky, and C. A. Scharf, Astrophys. J. **520**, 78 (1999).
[114] A. Finoguenov, T. H. Reiprich, and H. Böhringer, Astron. Astrophys. **368**, 749 (2001).
[115] H. Xu, G. Jin, and X.-P. Wu, Astrophys. J. **553**, 78 (2001).
[116] A. Del Popolo, F. Pace, and M. Le Delliou, J. Cosmol. Astropart. Phys. 03 (2017) 032.
[117] V. Antonuccio-Delogu and S. Colafrancesco, Astrophys. J. **427**, 72 (1994).
[118] A. Del Popolo, Astron. Astrophys. **454**, 17 (2006).
[119] S. D. M. White, Mon. Not. R. Astron. Soc. **174**, 19 (1976).
[120] A. Kashlinsky, Mon. Not. R. Astron. Soc. **208**, 623 (1984).
[121] A. Kashlinsky, Astrophys. J. **306**, 374 (1986).
[122] A. Kashlinsky, Astrophys. J. **312**, 497 (1987).